PCCP

PAPER

View Article Online
View Journal | View Issue

Cite this: *Phys. Chem. Chem. Phys.*, 2019, **21**, 9384

Role of the carbon source in the transformation of amorphous carbon to graphene during rapid thermal processing†

Xiaowei Li, *[ab] Yong Zhou,[b] Xiaowei Xu,[b] Aiying Wang[b] and Kwang-Ryeol Lee*[a]

Received 7th March 2019,
Accepted 8th April 2019

DOI: 10.1039/c9cp01305a

rsc.li/pccp

A fast transfer-free synthesis of a graphene structure can be successfully achieved by Ni-catalysed transformation of amorphous carbon (a-C) during rapid thermal processing, but the role of the a-C structure in the a-C-to-graphene transformation is still unclear. In this paper, the dependence of the transformation of a-C to graphene, the diffusion behaviour of C, and the graphene quality on the a-C structures was comparatively investigated by reactive molecular dynamics simulation and Ni was selected as a catalyst. The results demonstrated that different a-C structures affected the diffusion of C into Ni layers and the re-dissolving behaviour of the grown graphitic structures, and thus dominated the remnant number of C atoms, which played a critical role in the formation and quality of graphene.

Introduction

Amorphous carbon (a-C) with a mixture of 2-, 3-, and 4-coordinated carbon bonds is a large family of amorphous solid carbon structures,[1,2] which has attracted much attention in both scientific and engineering fields due to its excellent physicochemical properties.[3,4] In addition, it is an eco-friendly surface treatment technology, such as through physical vapor deposition and chemical vapor deposition (CVD), and can be achieved on various substrates at room temperature on a large scale, so it has been a strong candidate for protective coatings against mechanical or tribological failure of key components.[5,6]

Recent efforts[7–11] reported that in the presence of a catalytically active transition metal, a-C deposited on a dielectric surface could be successfully transformed into graphene by a rapid thermal processing (RTP) approach without the graphene post-transfer process. This breakthrough not only effectively releases the wrinkles, cracks, and contamination generated in the widely accepted mechanical exfoliation,[12] epitaxial growth,[13] liquid-phase exfoliation,[14] and CVD methods,[15] but also promotes the application of the a-C structure for the fast transfer-free synthesis of graphene on any dielectric substrate. However, it is well known that according to the fraction of hybridized structure, a-C can be divided into graphite-like carbon (GLC), tetrahedral a-C (ta-C) and so on;[16,17] the effects of different a-C structures on the diffusion behaviour of C atoms and the a-C-to-graphene transformation during the heating process were seldom considered in previous studies,[7–11,18] which is required for understanding the underlying transformation mechanism and guiding the preparation of graphene with high quality through the RTP method.

In our previous study,[19] the effects of different Ni surfaces ((100), (110), and (111)) as a catalyst on the diffusion behaviour of C into Ni and the graphene quality have been clarified, attributed to the difference in the diffusion activation energy. So in this work, we selected Ni(111) as a catalyst, and performed reactive molecular dynamics (RMD) simulations to demonstrate the dependence of the diffusion of a-C and its structural evolution on the a-C structures during the RTP process.

Computational methods

All calculations were conducted using the Large-scale Atomic/Molecular Massively Parallel Simulator code.[20] Two a-C structures, including one with a density of 3.22 g cm^{-3} (4-coordinated carbon fraction-63.3 at%, 3-coordinated carbon fraction-25.7 at%) known as ta-C and another with a density of 2.03 g cm^{-3} (4-coordinated carbon fraction-11.5 at%, 3-coordinated carbon fraction-66.5 at%) known as GLC, were selected as carbon sources, respectively, which had the same number of C atoms (872) and were obtained by *ab initio* molecular dynamics simulations using the liquid-quenching method. The detailed process was described in our previous work.[21] Ni(111) with a size of 29.902 × 25.896 × 12 Å^3 and

[a] *Computational Science Center, Korea Institute of Science and Technology, Seoul 136-791, Republic of Korea. E-mail: lixw0826@gmail.com, krlee@kist.re.kr*
[b] *Key Laboratory of Marine Materials and Related Technologies, Zhejiang Key Laboratory of Marine Materials and Protective Technologies, Ningbo Institute of Materials Technology and Engineering, Chinese Academy of Sciences, Ningbo 315201, P. R. China*

† Electronic supplementary information (ESI) available: Temperature selection for the a-C-to-graphene transformation; validation for the ReaxFF potential. See DOI: 10.1039/c9cp01305a

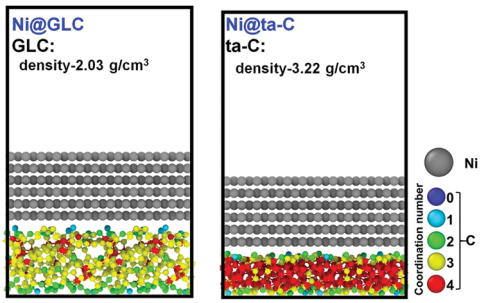

Fig. 1 Simulation models for the a-C-to-graphene transformation, which is composed of Ni(111) as a catalyst and different a-C structures including GLC and ta-C as carbon sources, respectively. The inset values are the density of each a-C structure. Gray balls correspond to Ni atoms, and blue, light blue, green, yellow, and red balls correspond to C atoms with different coordination numbers ranging from 0 to 4, respectively.

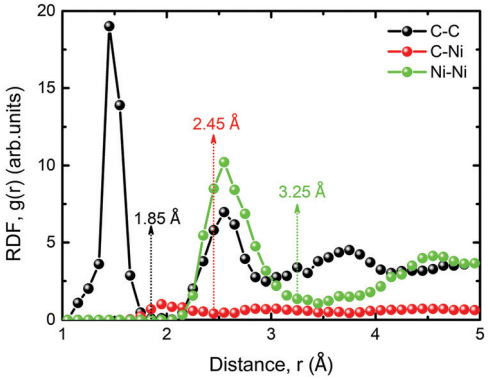

Fig. 2 RDF for C–C, C–Ni, and Ni–Ni interactions, where the inset values are the R_{cut} values for each bond, respectively.

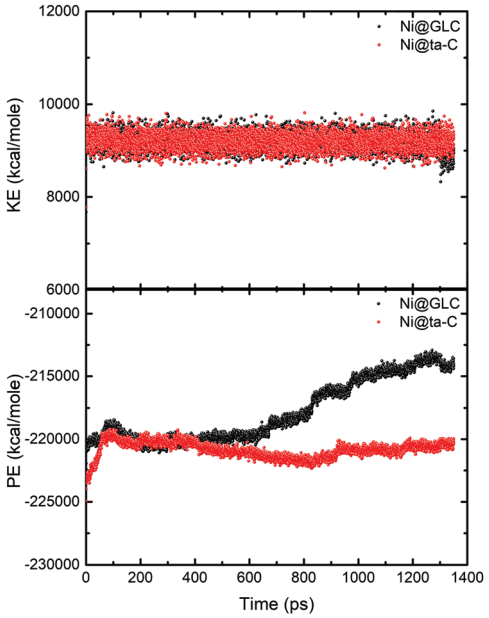

Fig. 3 Evolutions of the KE and PE as a function of diffusion time for the Ni@GLC and Ni@ta-C systems during diffusion at 1800 K for 1350 ps.

864 atoms was selected as a metal catalyst,[19] and the corresponding models (referred to as Ni@ta-C and Ni@GLC) can be found in Fig. 1. The average lattice mismatches between the Ni(111) and a-C models were 2.6% in the x direction and 0.6% in the y direction, respectively, and the initial separation distance between the Ni(111) and a-C layers was 3 Å. A vacuum space of 25 Å was applied on the top of the Ni surface, the time step was 0.25 fs, and periodic boundary conditions were applied along the x and y directions.

During the RTP process, there was no layer fixed in the whole simulation;[18] a stepwise heating strategy[19] (100 ps for each temperature) was adopted to raise the temperature from 300 to 1800 K in the *NVT* ensemble using a Nose–Hoover thermostat,[22] and then the Ni@a-C system was relaxed at 1800 K for 1350 ps to study the diffusion behaviour of C into the Ni layer during the short MD simulation time. The evolution of the mean square displacement (MSD), the hybridization structure of a-C, and the distributions of both C and Ni atoms with temperature (see the ESI,† Section S1) revealed that when the temperature was 1800 K, an obvious diffusion behaviour was realized in the Ni@a-C system without serious graphitic dissolution, but it was higher than those in previous experiments,[7–11] attributed to the absence of Ni defects or surface/interface contamination.

In addition, the cutoff radius, R_{cut}, of C–C, C–Ni, and Ni–Ni bonds was defined by the radial distribution function (RDF), and the first minimal values in RDF spectra were referred to as the criterion for judging whether the bond formed or not,[21] which were 1.85 Å for C–C, 2.45 Å for C–Ni, and 3.25 Å for Ni–Ni, respectively, as illustrated in Fig. 2. The ReaxFF potential developed by Mueller *et al.*[23] was used to describe the interaction between the C and Ni atoms, and the additional evaluation by RMD and *ab initio* calculations (see the ESI,† Section S2) confirmed its accuracy and reliability for the simulated system.

Results and discussion

Fig. 3 shows the evolution of the kinetic energy (KE) and potential energy (PE) as a function of diffusion time for different Ni@a-C systems at 1800 K. Note that for each case, the change in the KE with diffusion time is almost the same due to the same number of atoms and temperature. However, the significant difference in the PE with severe fluctuations suggests distinct structural evolution. Fig. 4 illustrates the MSD of C and Ni atoms during the RTP process at 1800 K for 1350 ps. From 0 to 600 ps, the MSD increases quickly, implying intermixing between the C and Ni atoms. In particular, the instantaneous diffusion of Ni into C is slightly faster than that of C into Ni owing to the constraint of strong C–C bonds. With further increasing the diffusion time up to 1350 ps, the MSD seems to be stabilized, indicating that a steady state is reached. Then, we select a short time (650–1350 ps) to calculate the diffusion coefficient, D, by the linear fitting of the MSD–time curves.[19] At 1800 K, the diffusion coefficients are found to be 2.0×10^{-7} for C and 5.5×10^{-8} cm^2 s^{-1} for Ni in the case of Ni@GLC, while they are 1.1×10^{-7} for C and 3.8×10^{-8} cm^2 s^{-1} for Ni in the case of Ni@ta-C, consistent with previous calculation[18] and

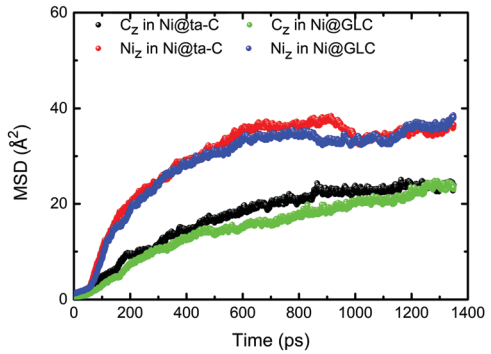

Fig. 4 MSD of C and Ni atoms with diffusion time for each case during the RTP process at 1800 K.

experimental values,[24] suggesting the viscous liquid character of the Ni–C mixing layer.

Fig. 5 displays the profiles of C and Ni atomic fractions along the diffusion couple direction and the corresponding morphologies of the Ni@GLC and Ni@ta-C systems at 1800 K, respectively. In each case, an atomic configuration showing a fuzzy C–Ni interface with locally mixed atoms is observed at 0 ps, but no distinct change is discernible in the structure. With the passage of time from 0 to 1350 ps, more atoms diffuse across the interface, thereby broadening the fuzzy interface, which eventually evolves into a wide diffusion zone (DZ) (gray regions in Fig. 5). The DZ has two borders or fronts, one bound by Ni (referred to as DZ-Ni) and the other by a-C (referred to as DZ-C). Because the diffusion coefficients of C and Ni in Ni@GLC are slightly higher than those in Ni@ta-C (Fig. 4), its DZ is wider than that of Ni@ta-C. Furthermore, at 1800 K, only a small number of Ni atoms diffuse into the a-C side at any specific diffusion time, whereas a significant number of C atoms move out of the a-C structure and diffuse into Ni, similar to the dissolution behaviour observed in Ni-catalysed CVD growth of graphene.[25,26] As a result, the initial interface broadens into a DZ and two moving interfaces or fronts with different velocities. The DZ-C front extends much more slowly with a small amount of Ni diffusing in and a large amount of C moving out as compared with the DZ-Ni front showing exactly opposite atomic movements. The two diffusion fronts, the slower DZ-C and faster DZ-Ni, clearly indicate asymmetric diffusion. As the asymmetric diffusion continues, the interface region enlarges, and the broadened DZ becomes more distorted. This is attributed to the introduction of C into Ni lowering the melting point of Ni and thus causing its structural transition.[9,18]

To further quantify the asymmetric diffusion process, the profiles for Ni@GLC are analysed (Fig. 5a): the width of the original interface is ~7.5 Å at 0 ps, and it increases gradually with the progression of time and reaches a final value of 25.6 Å at 1350 ps, as observed from the coordinates of the diffusion zone boundaries and fronts. The coordinate of the DZ-C front is changed by ~4.8 Å, while that of the DZ-Ni front is changed by 13.3 Å. For Ni@ta-C (Fig. 5b), the profiles reveal that, with the progress of time from 0 to 1350 ps, the width of the original interface grows from 6.3 to 22.3 Å with the coordinates of the DZ-C front changed by 2.2 Å and the DZ-Ni front changed by 13.7 Å. From these data, the average diffusion front velocities are estimated to be ~0.4 m s^{-1} for DZ-C and ~1.0 m s^{-1} for DZ-Ni in Ni@GLC, and ~0.2 m s^{-1} for DZ-C and ~1.0 m s^{-1} for DZ-Ni in Ni@ta-C. Note that although these velocities are average values, which are faster in the early stage and slower in the steady diffusion stage, these results reaffirm the aforementioned highly asymmetric diffusion.

Another intriguing observation is the appearance of a plateau in the concentration profiles of the two diffusing elements after 100 ps (light blue region in Fig. 5), which widens with time. Xiong *et al.*[9] also reported the formation of a nickel carbide (Ni_3C) phase at the interface between the Ni and a-C layers in experiment. However, we find that the Ni/C ratio is dependent on the diffusion time and a-C structure. The corresponding Ni/C atomic ratios in the plateau regions for the Ni@GLC system are

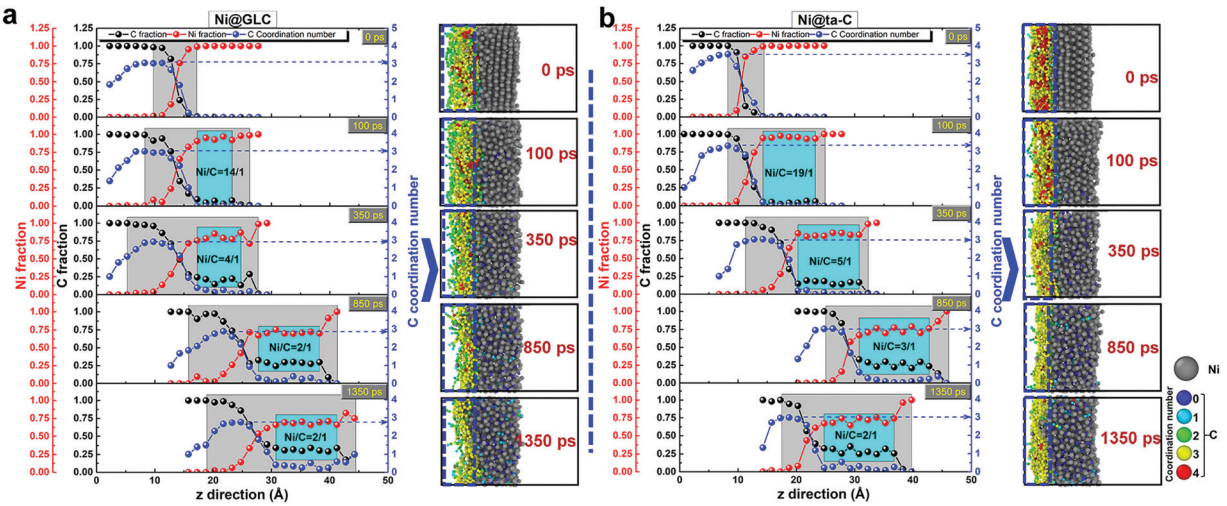

Fig. 5 Profiles of C and Ni atomic fractions and the coordination number of C along the diffusion couple direction and the corresponding morphologies in the (a) Ni@GLC and (b) Ni@ta-C systems, respectively.

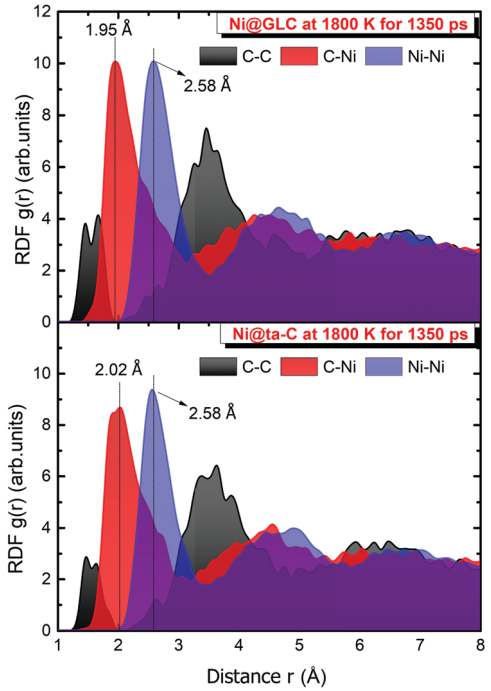

Fig. 6 RDF spectra of the plateau region in the Ni@GLC and Ni@ta-C systems, respectively, after diffusion at 1800 K for 1350 ps.

14/1 at 100 ps, 4/1 at 350 ps, 2/1 at 850 ps, and 2/1 at 1350 ps, while the corresponding values for Ni@ta-C are 19/1, 5/1, 3/1, and 2/1, respectively. The plateau marks a region of phase transition induced by inter-diffusion. Furthermore, the RDF of the plateau regions in Fig. 6 suggests a viscous liquid-like characteristic of the material, involving long-range disorder and short-range order.[18] The 1st peak positions of Ni–C and Ni–Ni interactions in the RDF spectra of Ni@GLC are located at 1.95 and 2.58 Å, respectively, while they appear to be at 2.02 and 2.58 Å, respectively, in Ni@ta-C.

In addition, RDF spectra are an effective tool to evaluate the structural transformation during the RTP process. It can be seen that following the diffusion time increasing from 0 to 1350 ps, the C–C RDF in the Ni@ta-C system (Fig. 7a) displays an amorphous character, but the peak intensity decreases gradually due to the diffusion of C atoms into Ni layers, and the 1st peak position deviates to 1.42 Å, which is related to the decrease of the bond length and the increase of the 3-coordinated C fraction, as will be discussed later; the peak intensity in the Ni–Ni RDF also decreases obviously with the diffusion time, suggesting the structural transformation of the Ni layer from crystalline to a liquid state[18,19] due to melting point depression. Because of the diffusion of C atoms into Ni layers, the peak intensity in the C–Ni RDF increases significantly. In the Ni@GLC system (Fig. 7b), the changes in the RDF spectra with diffusion time are similar to those in the Ni@ta-C system, except that the 1st peak position in the C–C RDF has no obvious change.

Considering the different changes in the 1st peak of the C–C RDF spectra for these two Ni@a-C systems (Fig. 7) and the contribution of the residual C atoms near the DZ-C front (dot-line regions in Fig. 5) to the graphene formation,[19] the corresponding change in hybridization with diffusion time is presented in Fig. 8. For Ni@ta-C, with the change in the diffusion time from 0 to 1350 ps, both the 1- and 2-coordinated C fractions remain almost constant, while the 3-coordinated C fraction increases obviously, due to the transformation of the 4-coordinated C structure catalysed by Ni,[18,19] which favours the formation of the graphene structure. However, in the case of Ni@GLC, the reduction in the 4-coordinated C fraction results in an increased fraction of dangling bonds rather than that of 3-coordinated C. This is

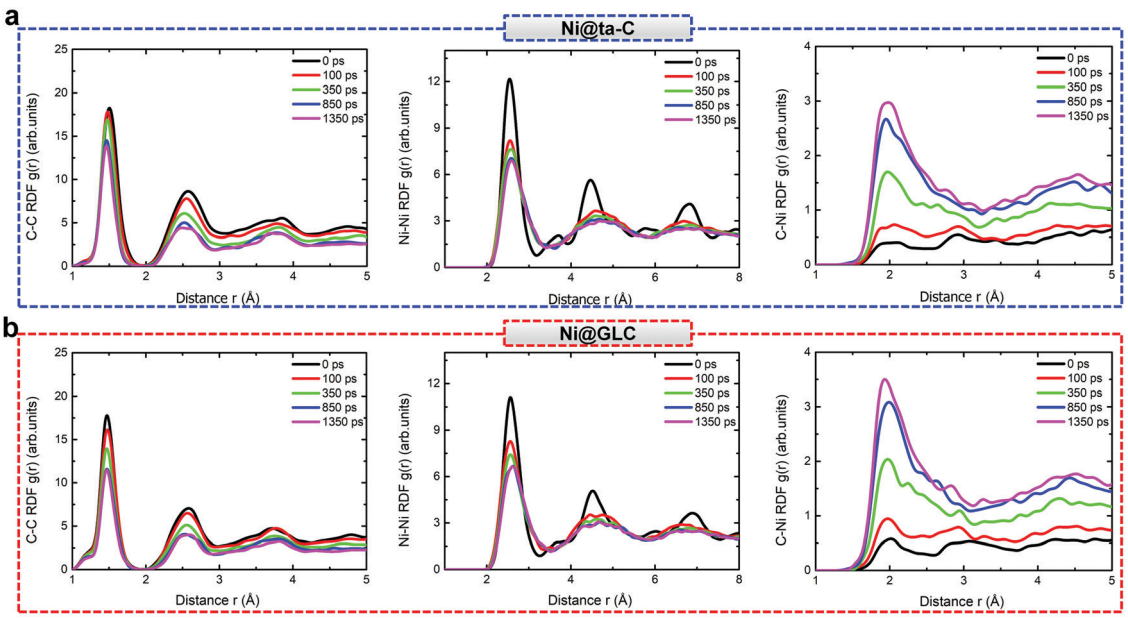

Fig. 7 RDF spectra with diffusion time in the (a) Ni@ta-C and (b) Ni@GLC systems, respectively, at 1800 K.

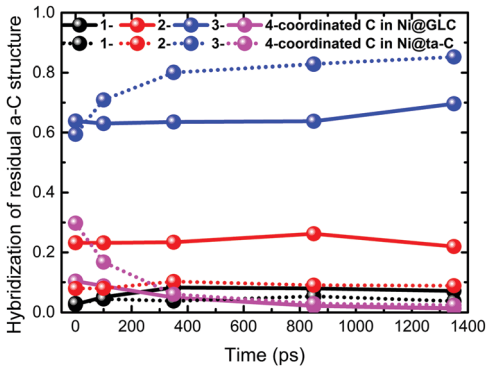

Fig. 8 Change in the hybridization of the residual a-C structures with diffusion time for each case.

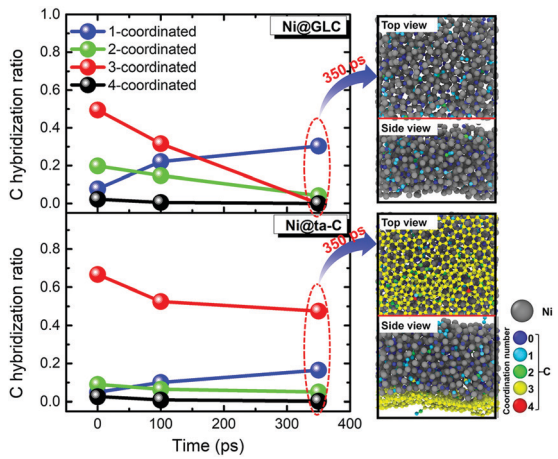

Fig. 9 Hybridization structure with diffusion time for all C atoms in the whole system for each case and the corresponding morphologies (top and side view) after diffusion at 2400 K for 350 ps.

because the high diffusion behaviour of C into the Ni layer induces the existence of re-dissolution of the graphitic structure, disfavouring the growth of high-quality graphene. This is more obvious as the temperature further increases up to 2400 K, as shown in Fig. 9. It can be seen that after diffusion at 2400 K for 350 ps, due to the re-dissolution of the graphitic structure into the Ni layer, the 3-coordinated C fraction in the Ni@GLC system reduces to 0, leading to the absence of the graphene structure. However, high-quality bilayer graphene is achieved in the Ni@ta-C system, although many excess graphitic structures also dissolve into Ni to form isolated or 1-coordinated C hybridized states. This suggests that compared with GLC, the ta-C structure with a high density and 4-coordinated C fraction is more suitable to realize the a-C-to-graphene transformation.

In order to comparatively evaluate the influence of different diffusion behaviour and structural transformation induced by the a-C structure on the grown graphene, Fig. 10 further shows the graphene structure generated in each case. Bilayer graphene is observed for Ni@ta-C. In contrast, the relatively higher D_{Ni} in Ni@GLC leads to a wider Ni–C intermixing layer and thus decreases the number of residual C atoms near the DZ-C front that are available to form a graphene structure. Further, the structural transformation from 4-coordinated C to 3-coordinated C is more obvious in Ni@ta-C than that in Ni@GLC; the 3-coordinated C fractions in the Ni@ta-C and Ni@GLC systems are found to be 85 at% and 70 at%, respectively (Fig. 10). Therefore, both the high number of C atoms and high 3-coordinated C fraction in Ni@ta-C promote the formation of a bilayer graphene structure with the presence of a Ni catalyst. Moreover, both the bond angle and length distributions of the generated graphene structures are evaluated. The same peak position (118°) of the bond-angle distribution (Fig. 10) is observed for each case. However, in Ni@ta-C,

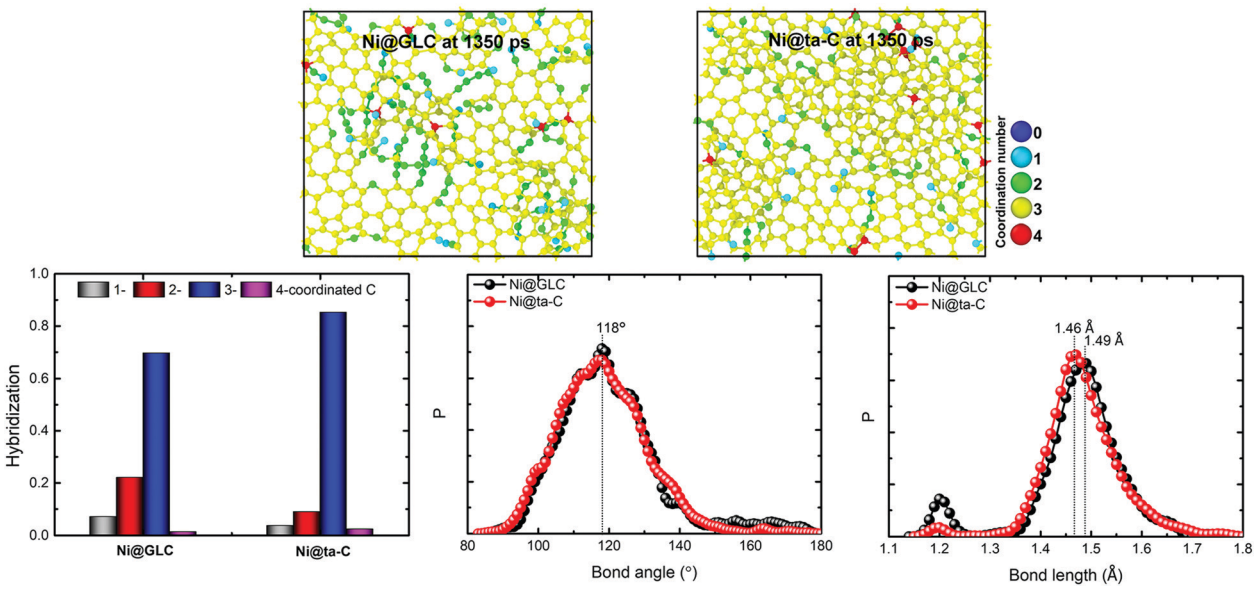

Fig. 10 Graphene structures obtained from the Ni@GLC and Ni@ta-C systems, respectively, after diffusion at 1800 K for 1350 ps, including the associated morphologies (the Ni and C atoms that diffuse into Ni layers are neglected for easy viewing), hybridization structure, and bond angle and length distributions.

the peak position of the bond-length distribution (1.46 Å) is closer to that of graphite (1.42 Å) than that of Ni@GLC (1.49 Å), and the intensity of the noise peak, located at a bond length of 1.2 Å, is also decreased significantly, originating from the reduced fractions of dangling bonds (2- and 1-coordinated C atoms in Fig. 10). This indicates the formation of a graphene structure with better quality when the a-C structure with a high density and high 4-coordinated C fraction is used as the carbon source.

It should be mentioned that the formation of the graphene structure using the RTP approach is obtained at high temperature, different to the dissolution/precipitation mechanism from the CVD method, but it can be explained by the Ni-induced crystallization and layer exchange mechanism reported by Chen[18] and Li,[19] and Ni also plays an important role to promote the dissolution or diffusion of surplus C atoms, stabilize the carbon dangling bonds, and catalyse the formation of a-C to graphene.[18] Moreover, compared with the experimental results, the graphene structures in our RMD simulations contain many holes and defects. This is attributed to the exceedingly faster rate of temperature increase in the present work than that in real experiments, causing the kinetics of graphene growth to be more dominant than the thermodynamics, leading to kinetically trapped defects in the structure.[18,19,27,28] In addition, the time for the a-C-to-graphene transformation in our calculations (1350 ps) is also much shorter than the experimental time. This fact explains the difference in the dimension of the system reported by Barreiro *et al.*[10] Therefore, defects present in the graphene structure could be healed if the simulation time is increased significantly[18] or upon high-temperature annealing,[27,28] which is confirmed by Fig. 9.

Conclusions

In conclusion, we explored the role of different a-C structures as carbon sources in the diffusion behaviours of C and Ni atoms and the Ni-catalysed a-C-to-graphene transformation through RMD simulation. Our results revealed that during the RTP process, the asymmetric diffusion of C and Ni atoms and the presence of a viscous liquid Ni–C intermixing layer were observed for each case. However, due to the lower diffusion coefficient of C in Ni@ta-C than that in Ni@GLC, a-C with a high 4-coordinated C fraction, such as ta-C, could undergo an obvious transformation from 4-coordinated C to 3-coordinated C, inducing a high fraction of the 3-coordinated C structure with low re-dissolution of the graphitic structure and a low fraction of dangling bonds, which promoted the formation of a graphene structure with high quality. This result sheds light on fundamental understanding of the effect of a-C structures on the a-C-to-graphene transformation, and guides the preparation and structural modification of graphene by tailoring the carbon source for a wide range of applications.

Conflicts of interest

There are no conflicts to declare.

Acknowledgements

This research was supported by the Korea Research Fellowship Program funded by the Ministry of Science and ICT through the National Research Foundation of Korea (2017H1D3A1A01055070), National Natural Science Foundation of China (51772307), and the Nano Materials Research Program through the Ministry of Science and IT Technology (NRF-2016M3A7B4025402).

Notes and references

1 J. Vetter, *Surf. Coat. Technol.*, 2014, **257**, 213–240.
2 L. Cui, Z. Lu and L. Wang, *Carbon*, 2014, **66**, 259–266.
3 L. Wang, L. Cui, Z. Lu and H. Zhou, *Carbon*, 2016, **100**, 556–563.
4 J. Huang, L. Wang, B. Liu, S. Wan and Q. Xue, *ACS Appl. Mater. Interfaces*, 2015, **7**, 2772–2783.
5 W. Dai, J. Liu, D. Geng, P. Guo, J. Zheng and Q. Wang, *Appl. Surf. Sci.*, 2016, **388**, 503–509.
6 W. Dai, F. Liu, J. C. Ding, Q. Wang and S. H. Kwon, *Diamond Relat. Mater.*, 2018, **87**, 107–114.
7 M. Zheng, K. Takei, B. Hsia, H. Fang, X. Zhang, N. Ferralis, H. Ko, Y. L. Chueh, Y. Zhang, R. Maboudian and A. Javey, *Appl. Phys. Lett.*, 2010, **96**, 063110.
8 J. A. Rodríguez-Manzo, C. Pham-Huu and F. Banhart, *ACS Nano*, 2011, **5**, 1529–1534.
9 W. Xiong, Y. S. Zhou, L. J. Jiang, A. Sarkar, M. Mahjouri-Samani, Z. Q. Xie, Y. Gao, N. J. Ianno, L. Jiang and Y. F. Lu, *Adv. Mater.*, 2013, **25**, 630–634.
10 A. Barreiro, F. Börrnert, S. M. Avdoshenko, B. Rellinghaus, G. Cuniberti, M. H. Rümmeli and L. M. K. Vandersypen, *Sci. Rep.*, 2013, **3**, 1115.
11 Z. Wu, Y. Guo, Y. Guo, R. Huang, S. Xu, J. Song, H. Lu, Z. Lin, Y. Han, H. Li, T. Han, J. Lin, Y. Wu, G. Long, Y. Cai, C. Cheng, D. Su, J. Robertson and N. Wang, *Nanoscale*, 2016, **8**, 2594–2600.
12 M. Yi and Z. Shen, *J. Mater. Chem. A*, 2015, **3**, 11700–11715.
13 S. Koh, Y. Saito, H. Kodama and A. Sawabe, *Appl. Phys. Lett.*, 2016, **109**, 023105.
14 J. Coelho, B. Mendoza-Sánchez, H. Pettersson, A. Pokle, E. K. McGuire, E. Long, L. McKeon, A. P. Bell and V. Nicolosi, *2D Mater.*, 2015, **2**, 025005.
15 G. Li, S. H. Huang and Z. Li, *Phys. Chem. Chem. Phys.*, 2015, **17**, 22832–22836.
16 J. Robertson, *Mater. Sci. Eng., R*, 2002, **37**, 129–281.
17 L. Zhang, X. Wei, Y. Lin and F. Wang, *Carbon*, 2015, **94**, 202–213.
18 S. Chen, W. Xiong, Y. S. Zhou, Y. F. Lu and X. C. Zeng, *Nanoscale*, 2016, **8**, 9746–9755.
19 X. Li, A. Wang and K. R. Lee, *Phys. Chem. Chem. Phys.*, 2019, **21**, 2271–2275.
20 S. Plimpton, *J. Comput. Phys.*, 1995, **117**, 1–19.
21 X. Li, P. Ke and A. Wang, *J. Phys. Chem. C*, 2015, **119**, 6086–6093.
22 D. J. Evans and B. L. Holian, *J. Chem. Phys.*, 1985, **83**, 4069–4074.
23 J. E. Mueller, A. C. T. van Duin and W. A. Goddard III, *J. Phys. Chem. C*, 2010, **114**, 4939–4949.

24 E. V. Rut'kov and N. R. Gall, *Equilibrium Nucleation, Growth, and Thermal Stability of Graphene on Solids, in Physics and Applications of Graphene – Experiments*, InTech, Rijeka, Croatia, 2011.
25 J. Gong, Z. Liu, J. Yu, D. Dai, W. Dai, S. Du, C. Li, N. Jiang, Z. Zhan and C. T. Lin, *Composites, Part A*, 2016, **87**, 290–296.
26 T. Wu, Z. Liu, G. Chen, D. Dai, H. Sun, W. Dai, N. Jiang, Y. H. Jiang and C. T. Lin, *RSC Adv.*, 2016, **6**, 23956–23960.
27 M. Jiao, W. Song, H. J. Qian, Y. Wang, Z. Wu, S. Irle and K. Morokuma, *Nanoscale*, 2016, **8**, 3067–3074.
28 S. Karoui, H. Amara, C. Bichara and F. Ducastelle, *ACS Nano*, 2010, **4**, 6114–6120.

